5-31-2011

Underwater Localization and Tracking of Physical Systems

Patrick E. Carroll
pec158@hotmail.com

Underwater Localization and Tracking of Physical Systems

by

Patrick Carroll

B.S. University of Connecticut, 2009

A Thesis

Submitted in Partial Fulfillment of the

Requirements for the Degree of

Master of Science

at the

University of Connecticut

2011

APPROVAL PAGE

Master of Sciences Thesis

Underwater Localization and Tracking of Physical Systems

Presented By

Patrick Carroll, B.S.

Major Advisor _____
Shengli Zhou

Associate Advisor _____
Jun-Hong Cui

Associate Advisor _____
Peter Willett

University of Connecticut

2011

Abstract

In this paper, we investigate the problem of localizing an underwater sensor node based on message broadcasting from multiple surface nodes. With the time-of-arrival measurements from a DSP-based multicarrier modem, each sensor node localizes itself based on the travel time differences among multiple senders to the receiver. Using one-way message passing, such a solution can scale to accommodate a large number of nodes in a network. We consider the issue from not only the physical layer, but also at the node processing layer by incorporating a tracking solution. We present simulation results as well as preliminary testing results in a swimming pool with both stationary and moving receivers.

I. Introduction

Underwater localization is a topic of great interest. Besides non-acoustic means, there are several localization baselines based on acoustic signaling. The first is the long base line (LBL) system, where transponders are installed at the sea floor, and the underwater vehicle interrogates the transponders for round-trip delay estimation followed by triangulation [1]. LBL has good localization accuracy, but it requires long-time calibration. The second is the short base line (SBL) system, where a mother-ship moves above the underwater vehicle. The ship locates the vehicle using a high-frequency directional emitters. The third approach is based on floating buoys [2], [3]. This system acts like a long base line system except that the reference points are surface buoys. There are commercial products – the GPS Intelligent Buoys (GIB) – that route signals from an underwater node to surface buoys [2], and using radio links the surface buoys forward all information to a mother-ship, wherein the localization is performed. The floating buoys are easier to deploy and calibrate than LBL systems.

In this paper, we propose a new localization approach based on message broadcasts from multiple surface nodes, coupled with tracking algorithms and implemented on a physical system to provide a complete analysis.

With the time-of-arrival measurements, the receiver computes its own localization based on the differences of the travel time among multiple senders to the receiver. We present one solution based on exhaustive search, and the other based on the least-squares formulation [7]. By implementing the localization algorithms in the OFDM modem prototypes developed in [4], we have carried out tests in a swimming pool. With these point measurements,

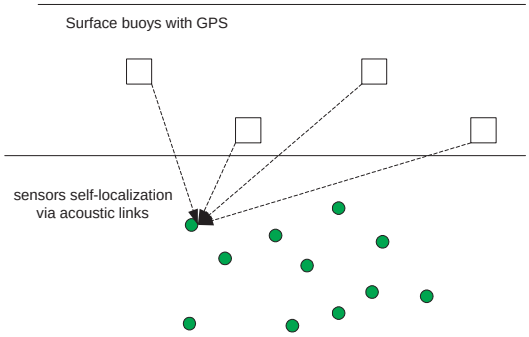

Fig. 1. An underwater sensor network with multiple surface buoys.

tracking analysis was also carried out on the pool data obtained by the modems.

Thus we consider the problem not only in terms of the physical layer at the modem with timing and detection, but further analyze analyze it in a single point estimate, and ultimately combine the point estimates for a tracking implementation. In particular we consider two particular tracking scenarios: a largely static scenario in which the nodes are assumed to be tethered or freely floating with no self-propulsion methods, and a mobile scenario in which the object being tracked is assumed to make deliberate maneuvers and have full control of its motion, such as an AUV.

The advantage of the proposed localization method is that the broadcast messages can serve an arbitrary number of underwater nodes once they are in range, in contrast to existing solutions which can only serve a small number of users.

The rest of the paper is organized as follows. We present the system overview in Section II. Sections IV and V contain simulation results and testing results in a swimming pool respectively. Conclusions are in Section VI.

II. System Overview

Fig. 1 depicts the considered system setup, with several surface nodes and multiple underwater nodes. The surface nodes are equipped with satellite-based GPS receivers. Relying on the interval pulse provided by the GPS device that is accurate to within 1 microsecond GPS time, the surface nodes are well synchronized. At predetermined intervals, the surface nodes sequentially broadcast their current location and time.

The underwater nodes within the broadcast range will hear a series of transmissions and decode those messages. By comparing the reception time with the transmission time

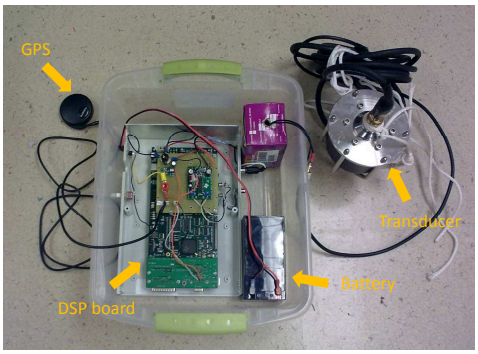

Fig. 2. The OFDM modem prototype with an attached GPS unit

encoded in the message, each underwater node can obtain estimates of the time-of-arrivals (or time-of-flights) of messages from different surface nodes, based on which it tries to compute its own position. Note that the broadcast from the surface to underwater nodes is one-way transmission, that localization quality is independent of the number of underwater nodes in the network, and that there is no additional interference involved among different underwater nodes.

Let us focus on one receiver at position (x_r, y_r, z_r). Suppose that there are N surface nodes, at positions (x_n, y_n, z_n), $n = 1, \ldots, N$. Let d_n denote the distance between the receiver node and the nth surface node:

$$d_n = \sqrt{(x_r - x_n)^2 + (y_r - y_n)^2 + (z_r - z_n)^2}. \tag{1}$$

Without loss of generality, we set the first surface node at the origin, i.e., $x_1 = y_1 = z_1 = 0$, such that

$$d_1^2 = x_r^2 + y_r^2 + z_r^2. \tag{2}$$

The actual time of arrival is $t_n = d_n/c$, where c is the sound propagation speed.

The receiver needs to provide an estimate on the time of arrival t_n. In this paper, we use real-time DSP-based OFDM modem prototypes [4], as shown in Fig. 2, which implements the coarse synchronization algorithm developed in [5]. After coarse synchronization, the OFDM preamble is decoded to generate an estimate of the channel impulse response, and the first arrival is detected via the modified Page test as in [6].

First, the channel is observed to detect when a signal appears, based on a background noise level monitoring performed by the modem at initialization. When a signal is detected,

the correlation of the signal with a sliding window of itself is compared to determine the level of peak correlation in the pre-amble of the message occurs, indicated by a plateau in the correlation. Once this plateau is selected, the time of arrival is coarsely estimated as having been approximately halfway during this plateau period. Once coarse channel estimation has occurred, the preamble, which entirely known to the receiver, is used to estimate the instantaneous underwater channel conditions, and from there, a more refined estimation of the time of arrival is performed [4].

Once a node collects several timing messages, it can form a single point estimate of its current position. This is accomplished by way of localization algorithms based on the intersection of spherical surfaces.

Let $\hat{t}_n$ denote the estimate of t_n from the OFDM modem. It can be expressed as the sum of the real transmission propagation, the delay in signal processing at both transmitter and receiver, and the estimation noise w_n

$$\hat{t}_n = t_n + b_n + w_n. \tag{3}$$

Multiple tests of the OFDM modem reveal that the noise w_n has variance on the order of $5 - 10\,ms$. On the other hand, the processing delay (bias) b_n has large magnitude, which might be on the order of $500\,ms$. However, tests have also shown that b_n is nearly identical across modems with similar hardware operating with the same software and GPS synchronization. Thus, we will treat b_n as a constant $b_n = b$ in the sequel, and present the localization algorithms based on

$$\hat{t}_n = t_n + b + w_n, \quad n = 1, \ldots, N. \tag{4}$$

Since the bias b is unknown and usually large, time-of-arrival (TOA) based methods are not suitable. Instead, we use the time-difference-of-arrival (TDOA) method to cancel the common bias term b by forming

$$\Delta\hat{t}_{n1} = \hat{t}_n - \hat{t}_1, \quad n = 2, \ldots, N. \tag{5}$$

The distance difference $d_{n1} = d_n - d_1$ is then estimated by

$$\hat{d}_{n1} = c\Delta\hat{t}_{n1}. \tag{6}$$

The TDOA method also corrects for clock skew alongside this bias term, due to the nature of the shared GPS clock. Each recieving node will have its own internal clock,

which at some update period k will have drifted by an unknown, non-linear skew factor $\phi(k)$. Each of the surface transmitters, however, will have the same clock skew, and due to the periodic corrections by the gps clock, this value should be approximately 0 for any period k. Thus, each transmission time can be represented as

$$\hat{t}_n = t_n + b + \phi(k) + w_n, \quad n = 1, \ldots, N. \tag{7}$$

and again, by taking the difference of the time-of-arrival estimates, this common clock skew is eliminated from the timing estimate.

Next we present the localization methods based on the exhaustive search and least-squares formulations.

A. Exhaustive Search

The individual time estimates $\hat{t}_n$ generally have correlated noise in the underwater channel. For simplicity, we assume instead that they are independent and identically distributed, and pursue a maximum likelihood function.

$$\min_{x_r, y_r, z_r} f(x_r, y_r, z_r) = \sum_{n=2}^{N} (c\Delta\hat{t}_{n1} - (d_n - d_1))^2. \tag{8}$$

The solution to (8) is found by exhaustive search.

In the presence of colored noise, a correlated measurement modification can be made as follows:

$$\min_{x_r, y_r, z_r} f(x_r, y_r, z_r) = (\Delta\underline{\hat{t}} - \Delta\underline{d})^T P^{-1} (\Delta\underline{\hat{t}} - \Delta\underline{d}). \tag{9}$$

where

$$\Delta\underline{\hat{t}} = \begin{bmatrix} \Delta\hat{t}_{21} \\ \Delta\hat{t}_{31} \\ \vdots \\ \Delta\hat{t}_{n1} \end{bmatrix} \quad \Delta\underline{d} = \begin{bmatrix} d_2 - d_1 \\ d_3 - d_1 \\ \vdots \\ d_n - d_1 \end{bmatrix}$$

and P is an nxn covariance matrix

$$P = \begin{bmatrix} 1 & 1/2 & 1/2 & \ldots & 1/2 \\ 1/2 & 1 & 1/2 & \ldots & 1/2 \\ \vdots & \vdots & \vdots & \ldots & \vdots \\ 1/2 & 1/2 & 1/2 & \ldots & 1 \end{bmatrix} \tag{10}$$

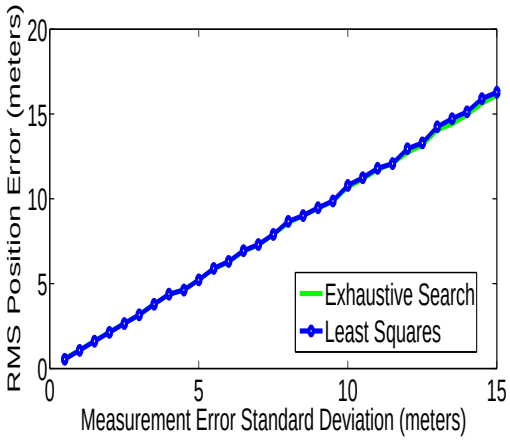

Fig. 3. Root-mean-squared (RMS) localization error as a function of the standard deviation of the distance measurements.

B. Least Squares Solution

We use the least-squares solution from [7]. Since $d_n = d_{n1} + d_1$, we have

$$(d_{n1} + d_1)^2 = x_n^2 + y_n^2 + z_n^2 - 2x_n x_r - 2y_n y_r - 2z_n z_r + d_1^2, \tag{11}$$

which can be simplified as

$$x_n x_r + y_n y_r + z_n z_r = \frac{1}{2}(\left[x_n^2 + y_n^2 + z_n^2 - d_{n1}^2\right]) - d_{n1} d_1. \tag{12}$$

Define the following matrix and vectors

$$\mathbf{H} = \begin{bmatrix} x_2 & y_2 & z_2 \\ x_3 & y_3 & z_3 \\ \vdots & \vdots & \vdots \\ x_N & y_N & z_N \end{bmatrix}, \quad \mathbf{v} = \begin{pmatrix} -\hat{d}_{21} \\ -\hat{d}_{31} \\ \vdots \\ -\hat{d}_{N1} \end{pmatrix} \tag{13}$$

$$\mathbf{u} = \frac{1}{2}\begin{bmatrix} x_2^2 + y_2^2 + z_2^2 - \hat{d}_{21}^2 \\ x_3^2 + y_3^2 + z_3^2 - \hat{d}_{31}^2 \\ \vdots \\ x_N^2 + y_N^2 + z_N^2 - \hat{d}_{N1}^2 \end{bmatrix}, \quad \mathbf{a} = \begin{bmatrix} x_r \\ y_r \\ z_r \end{bmatrix}. \tag{14}$$

The least-squares solution can be obtained as

$$\hat{\mathbf{a}} = d_1 \mathbf{H}^\dagger \mathbf{v} + \mathbf{H}^\dagger \mathbf{u}, \tag{15}$$

where $\dagger$ stands for pseudo-inverse. Substituting the entries of $\hat{\mathbf{a}}$ into (2) yields a quadratic equation for d_1 [7]. Solving for d_1 and substituting the positive root back into (15) provides the final solution for the receiver position $\mathbf{a}$.

III. Tracking Algorithms

From a single point measurement, the localization error can be quite large, and thus in order to reduce the error tracking algorithms can be implemented in order to combine the knowledge of multiple measurements into a more accurate position estimate.

In order to consider which tacking approach would be best is to first consider the scenario in which the node is being localized. There are two distinct modes in which underwater nodes move: either passively, with the water currents as a free-floating node, or actively as an underwater vehicle such as an AUV. Both are characterized primarily by long periods of relatively straight motion at a slowly-changing speed. Typically, AUV motion differs in that at certain random intervals, it will change direction according to operator instruction. Most search patterns for AUVs are defined by spiral paths, or by rectangular search grids. In either case, the vehicle is likely to alter its direction by way of a continuous turn; that is, to make a turn at a fixed angular velocity until the desired heading is achieved (or in the case of a spiral, until the search area is exhausted).

A. Kalman Filter

In the KF, we chose to model the movement of the node as set of discrete white noise acceleration models, with a separate model for each possible direction; that is, x, y and z. As such, the state equation for the Kalman filter at time index $k+1$ based on information from time step k becomes

$$L(k+1) = \mathbf{F}(k)L(k) + v(k) \tag{16}$$

with measurement

$$z(k+1) = \mathbf{H}(k+1)L(k+1) + w(k+1) \tag{17}$$

where

$$\mathbf{F} = \begin{bmatrix} 1 & \tau & 0 & 0 & 0 & 0 \\ 0 & 1 & 0 & 0 & 0 & 0 \\ 0 & 0 & 1 & \tau & 0 & 0 \\ 0 & 0 & 0 & 1 & 0 & 0 \\ 0 & 0 & 0 & 0 & 1 & \tau \\ 0 & 0 & 0 & 0 & 0 & 1 \end{bmatrix} \tag{18}$$

$$\mathbf{H} = \begin{bmatrix} 1 & 0 & 0 & 0 & 0 & 0 \\ 0 & 0 & 1 & 0 & 0 & 0 \\ 0 & 0 & 0 & 0 & 1 & 0 \end{bmatrix} \tag{19}$$

$v(k)$ is process noise, $w(k)$ is measurement noise and τ is the sampling interval of the discrete model in seconds.

The state covariance is modeled as

$$\mathbf{P}(k+1|k) = \mathbf{F}(k)\mathbf{P}(k|k)\mathbf{F}(k)^T + \mathbf{Q}(k) \tag{20}$$

The corresponding process noise has a covariance given as:

$$\mathbf{Q} = \begin{bmatrix} \frac{1}{4}\tau^4 & \frac{1}{2}\tau^3 & 0 & 0 & 0 & 0 \\ \frac{1}{2}\tau^3 & \tau^2 & 0 & 0 & 0 & 0 \\ 0 & 0 & \frac{1}{4}\tau^4 & \frac{1}{2}\tau^3 & 0 & 0 \\ 0 & 0 & \frac{1}{2}\tau^3 & \tau^2 & 0 & 0 \\ 0 & 0 & 0 & 0 & \frac{1}{4}\tau^4 & \frac{1}{2}\tau^3 \\ 0 & 0 & 0 & 0 & \frac{1}{2}\tau^3 & \tau^2 \end{bmatrix} \sigma_v^2 \tag{21}$$

Here, σ_v is a design parameter that is chosen to match the most likely level of process noise to be experienced by the object in question; which is to say it controls how much the model anticipates the object to maneuver. Given that the object in question is likely to be either stationary or altering its velocity at a slow, steady rate, a process noise level of $\sigma_v = 0.5\,\mathrm{m/s^2}$ was selected to best emulate this behavior. The filter was initialized with two-point differencing.

B. Interacting Multiple Model Filter

For the more complex motion of an active underwater node, an Interacting Multiple Model filter (IMM) was implemented, as the expected maneuvering index of underwater vehicles, can easily exceed the threshold for which a single linear filter is likely to have any benefit. To this end, the IMM was a simple two-model filter, with a single, linear, low process noise ($\sigma_v = 0.05\,\mathrm{m/s^2}$) KF to account for the straight motion travel, and an extended Kalman filter (EKF), configured in a coordinated-turn mode [9]. This validity of the coordinated turn assumption is dependent on the scenario in question, though given the previously described search patterns, it should be sufficiently accurate [8].

The linear KF uses similar system equations as given previously, augmented with an additional column and row of zeros in order to accommodate the use of the EKF's additional state in the IMM. The EKF in this problem uses one of two sets of state equations: the first set is an approximation used when the predicted coordinated turn rate is near 0 ($\hat{\Omega}(k) \approx 0$), and the second set is used when the predicted coordinated turn rate is greater than some detection threshold ($|\hat{\Omega}(k)| > 0$) [10].

The first set of EKF state equation modifications ($\hat{\Omega}(k) \approx 0$) is as follows:

$$\mathbf{F}_L(k) = \begin{bmatrix} 1 & \tau & 0 & 0 & 0 & 0 & -\frac{1}{2}\tau^2\hat{\dot{\eta}}(k) \\ 0 & 1 & 0 & 0 & 0 & 0 & -\tau\hat{\dot{\eta}}(k) \\ 0 & 0 & 1 & \tau & 0 & 0 & \frac{1}{2}\tau^2\hat{\dot{\xi}}(k) \\ 0 & 0 & 0 & 1 & 0 & 0 & \tau\hat{\dot{\xi}}(k) \\ 0 & 0 & 0 & 0 & 1 & \tau & 0 \\ 0 & 0 & 0 & 0 & 0 & 1 & 0 \\ 0 & 0 & 0 & 0 & 0 & 0 & 1 \end{bmatrix} \tag{22}$$

where η and ξ represent the x and y directions, respectively, and we denote $\dot{\eta}$ as the velocity component in the η direction.

When $|\hat{\Omega}(k)| > 0$,

$$\mathbf{F}_L(k) = \begin{bmatrix} 1 & \frac{\sin\hat{\Omega}(k)}{\hat{\Omega}(k)}\tau & 0 & -\frac{1-\cos\hat{\Omega}(k)\tau}{\hat{\Omega}(k)} & 0 & 0 & f_{\Omega,1(k)} \\ 0 & \cos\hat{\Omega}(k)\tau & 0 & -\sin\hat{\Omega}(k)\tau & 0 & 0 & f_{\Omega,2(k)} \\ 0 & \frac{1-\cos\hat{\Omega}(k)\tau}{\hat{\Omega}(k)} & 1 & \frac{\sin\hat{\Omega}(k)\tau}{\hat{\Omega}(k)} & 0 & 0 & f_{\Omega,3(k)} \\ 0 & \sin\hat{\Omega}(k)\tau & 0 & \cos\hat{\Omega}(k)\tau & 0 & 0 & f_{\Omega,4(k)} \\ 0 & 0 & 0 & 0 & 1 & \tau & 0 \\ 0 & 0 & 0 & 0 & 0 & 1 & 0 \\ 0 & 0 & 0 & 0 & 0 & 0 & 1 \end{bmatrix} \tag{23}$$

where the partial derivatives $f_{\Omega,1(k)}, ...f_{\Omega,4(k)}$ are found as:

$$\begin{bmatrix} f_{\Omega,1(k)} \\ f_{\Omega,2(k)} \\ f_{\Omega,3(k)} \\ f_{\Omega,4(k)} \end{bmatrix} = \begin{bmatrix} \frac{(\cos\hat{\Omega}(k)\tau)\tau\hat{\dot{\xi}}(k)}{\hat{\Omega}(k)} - \frac{(\sin\hat{\Omega}(k)\tau)\hat{\dot{\xi}}(k)}{\hat{\Omega}(k)^2} - \frac{(\sin\hat{\Omega}(k)\tau)\tau\hat{\dot{\eta}}(k)}{\hat{\Omega}(k)} - \frac{(-1+\cos\hat{\Omega}(k)\tau)\hat{\dot{\eta}}(k)}{\hat{\Omega}(k)^2} \\ -(\sin\hat{\Omega}(k)\tau)\tau\hat{\dot{\xi}}(k) - (\cos\hat{\Omega}(k)\tau)\tau\hat{\dot{\eta}}(k) \\ \frac{(\sin\hat{\Omega}(k)\tau)\tau\hat{\dot{\xi}}(k)}{\hat{\Omega}(k)} - \frac{(1-\cos\hat{\Omega}(k)\tau)\hat{\dot{\xi}}(k)}{\hat{\Omega}(k)^2} + \frac{(\cos\hat{\Omega}(k)\tau)\tau\hat{\dot{\eta}}(k)}{\hat{\Omega}(k)} - \frac{(\sin\hat{\Omega}(k)\tau)\hat{\dot{\eta}}(k)}{\hat{\Omega}(k)^2} \\ (\cos\hat{\Omega}(k)\tau)\tau\hat{\dot{\xi}}(k) - (\sin\hat{\Omega}(k)\tau)\tau\hat{\dot{\eta}}(k) \end{bmatrix} \tag{24}$$

In both cases, the process noise covariance is determined in the following state equations:

$$\mathbf{P}(k+1|k) = \mathbf{F}_L(k)\mathbf{P}(k|k)\mathbf{F}_L(k)' + \Gamma\text{EKF}\mathbf{Q}(k)\Gamma'_{\text{EKF}}$$

where

$$\Gamma_{\text{EKF}} = \begin{bmatrix} \frac{1}{2}\tau^2 & 0 & 0 & 0 \\ \tau & 0 & 0 & 0 \\ 0 & \frac{1}{2}\tau^2 & 0 & 0 \\ 0 & \tau & 0 & 0 \\ 0 & 0 & \frac{1}{2}\tau^2 & 0 \\ 0 & 0 & \tau & 0 \\ 0 & 0 & 0 & \tau \end{bmatrix} \tag{25}$$

From our assumptions of AUV motion, the value of Q(k) was selected as:

$$\mathbf{Q}(k) = \begin{bmatrix} (1.25\,\text{m/s}^2)^2 & 0 & 0 & 0 \\ 0 & (1.25\,\text{m/s}^2)^2 & 0 & 0 \\ 0 & 0 & (1.25\,\text{m/s}^2)^2 & 0 \\ 0 & 0 & 0 & (0.3 * \pi/180\,\text{rad})^2 \end{bmatrix} \tag{26}$$

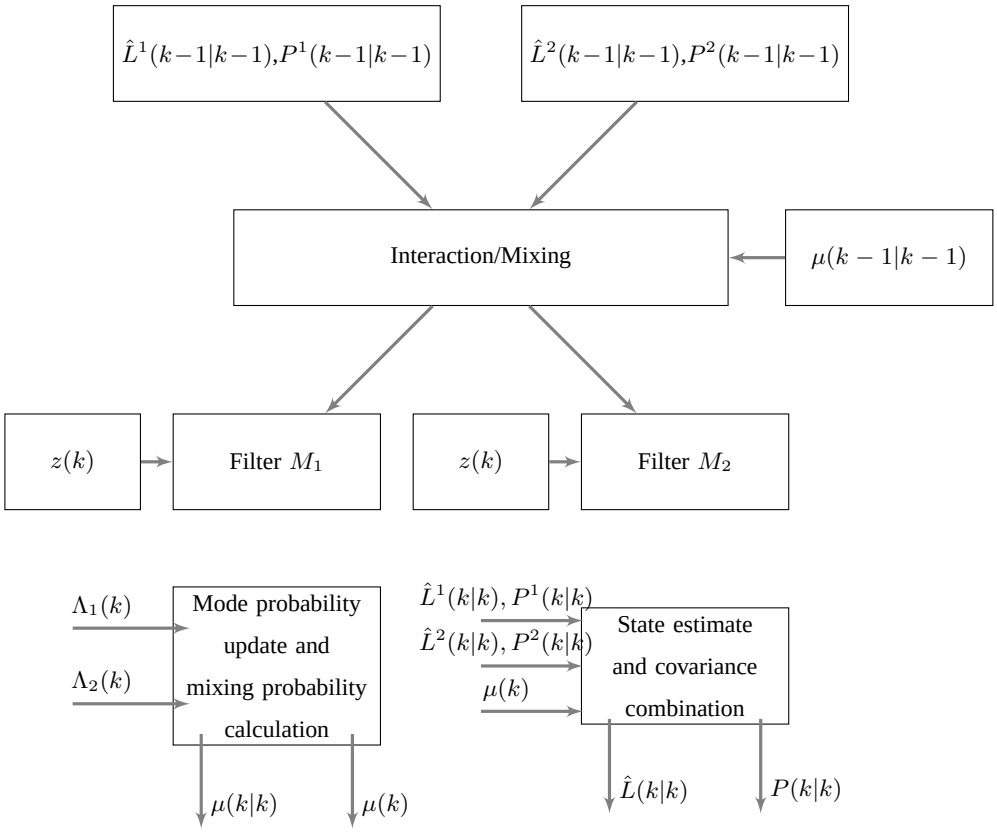

Fig. 4. IMM-CT block diagram for a single measurement update [10]

The IMM-CT is outlined in Fig. 4. The linear KF is designed as described previously, whereas the non-linear EKF has a different set of model selection parameters which define how it interprets large differences in the measurements. In this case, it is a covariance matrix that controls the rate of change. In particular, it describes how much variation occurs during the coordinated maneuver in terms of the angular velocity, and as such as two directional speed components and a angle change component.

IV. Simulation Results

We first carry out simulation using a simple noise model to generate the TOA measurements and evaluate the localization accuracy. For simplicity, z is assumed to be known, and we only solve for x and y coordinates. Four transmitters are placed on a square grid with coordinates $(0, 0)$, $(100, 0)$, $(0, 100)$, and $(100, 100)$. One receiver is placed at the center between the origin and the $(0, 100)$ point, and moves at a constant rate of 0.125 m/s parallel to the x-axis.

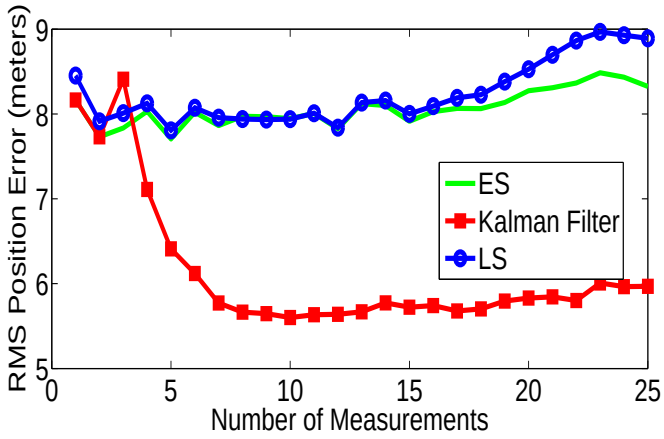

Fig. 5. Root-mean-squared (RMS) localization error as a function of the number of measurements acquired as the receiver moved in a straight line

The TOAs are generated according (3) where b is a fixed large bias, and w_n is i.i.d. zero-mean white Gaussian noise with standard deviation of 7.5 m. Position updates were taken every 16 seconds.

The localization position error is shown in Fig. 5 as a function of range measurement errors. We see that the LS solution has similar performance as the exhaustive search. We have also tried to change the clock bias, which has almost no effect upon the position error, as expected.

An additional set of simulated data compares the Kalman Filter's performance for various levels of measurement noise, with results given in Fig. 6. As the measurement noise increased, the error floor of the Kalman Filter increased, however, the level of improvement over the raw measurements also increased.

A third set of simulations examined the affect of the speed of the tracked object on the Kalman Filter's ability to estimate the object's position. To test this, the same node position and update interval were observed as in the original scenarios, however the speed was varied from 0.125 m/s to 0.5 m/s parallel to the x-axis.

In addition to the Kalman filter, simulations for the proposed IMM-CT were also run, using the relatively challenging scenario presented in Fig. 7, with the corresponding RMS position error given by Fig. 8.

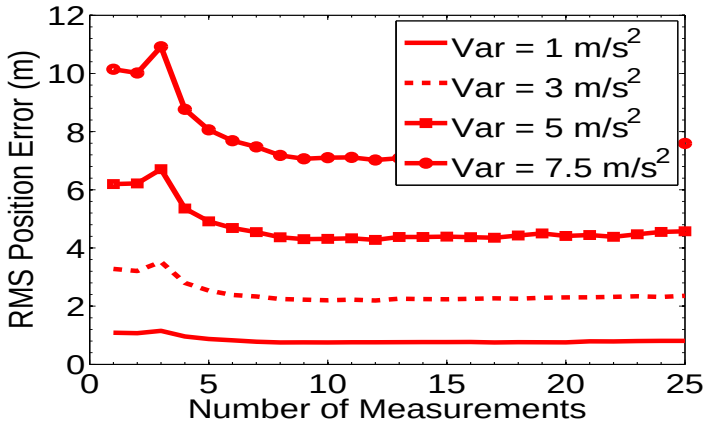

Fig. 6. Root-mean-squared (RMS) localization error as a function of the number of measurements acquired as the receiver moved in a straight line

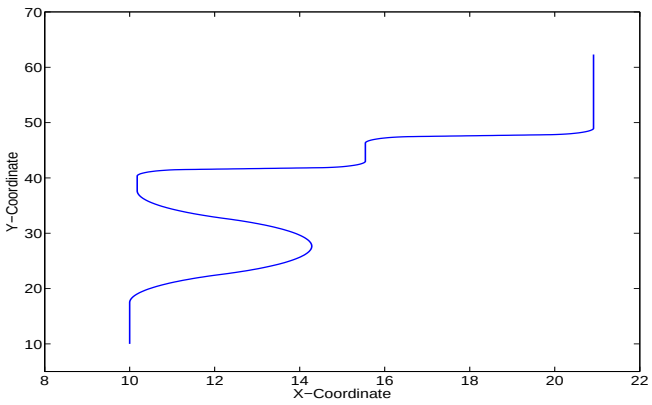

Fig. 7. Simulation path for the IMM-CT, with distances in meters.

V. Pool Tests

We carried out tests in a standard competitive athletic swimming pool at University of Connecticut, Storrs, whose dimensions are perfectly known. These tests did not use the GPS capabilities of the nodes, due to the limitation of the GPS receivers indoors. The nodes were fixed to the corner locations of the pool, such that their locations are measured accurately. The receiver was positioned approximately in the center of the pool, as outlined in Fig. 9. All the transducers are placed about 1 m below the surface. The pool has a depth about 3 m. Stationary tests were conducted during March 2010 and April 2011 while the mobile test was conducted during December 2010.

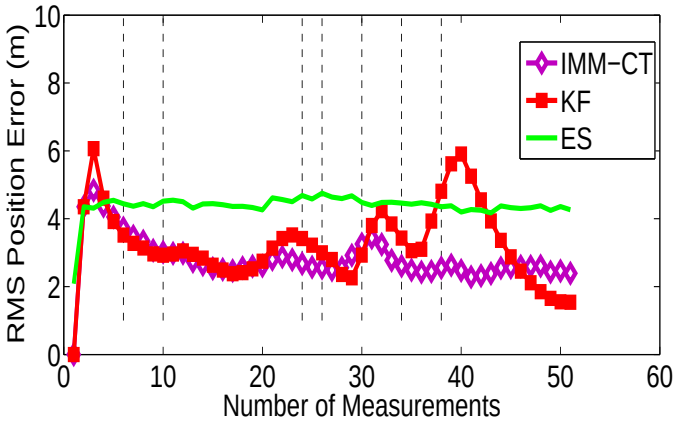

Fig. 8. Root-mean-squared (RMS) localization error as a function of the number of measurements acquired as the receiver moved in the scenario.

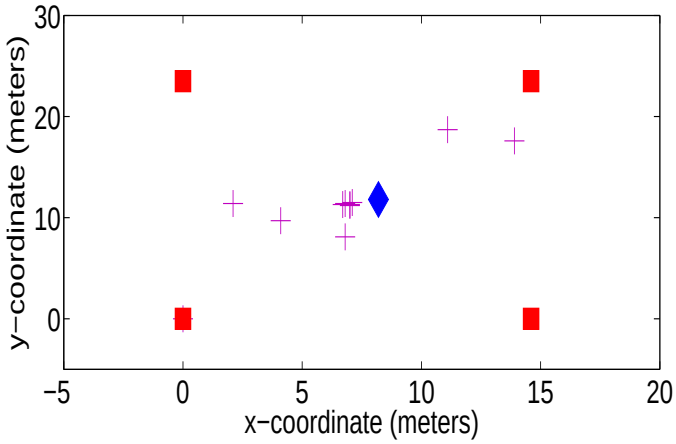

Fig. 9. Node deployment during March 2010 pool test. The transmitters are denoted by squares, and the receiver is denoted by the diamond. The scattered plus signs are the estimates by the exhaustive search method.

A. Test Case 1

(Stationary test, March 2010)

During the test, not all the messages from the transmitters were decoded correctly. For this reason, we use the data set with at least three measurements within one cycle of broadcasting from the four surface nodes. The favorable geometry and the known value of z allow an estimate based on only three surface nodes. The location estimates by the exhaustive search method are shown in Fig. 9, and those by the LS method shown in Fig. 10. We see that the LS estimates from these data sets are biased.

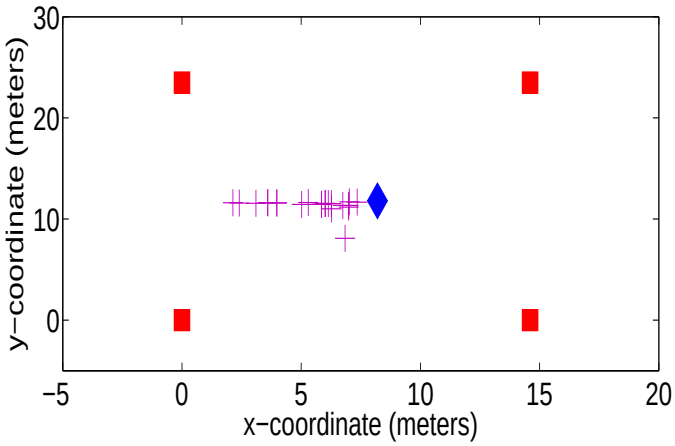

Fig. 10. Node deployment during March 2010 pool test. The transmitters are denoted by squares, and the receiver is denoted by the diamond. The scattered plus signs are the estimates by the least-squares method.

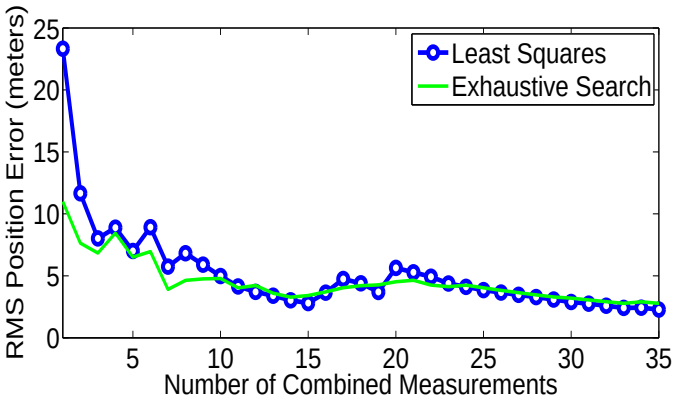

Fig. 11. Localization error during March 2010 pool test.

Although advanced algorithms could be applied to fuse the data from multiple data sets, here we simply average the location estimates from multiple data sets. As more data sets are available, the localization accuracy improves, as shown in Fig. 11. A localization error of about 5 m is achieved with about 10 data sets.

B. Test Case 3

(Stationary test, April 2011)

During the test, all the messages from a single node were not decoded correctly. For this reason, we use the data set consisting only of transmissions from the remaining three

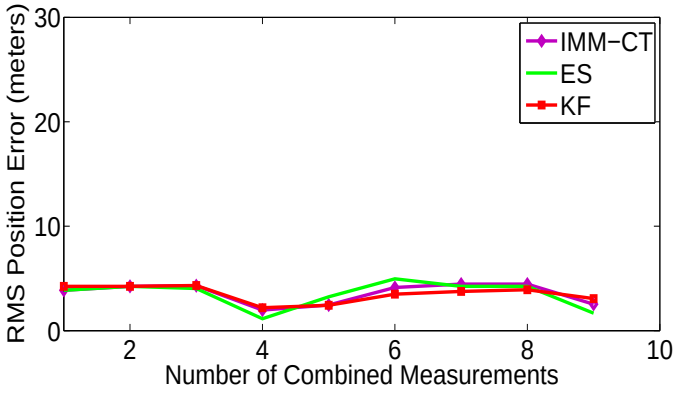

Fig. 12. Localization error during April 2011 pool test.

nodes. By using the known value of z, we were able to reduce the minimum number of equations needed to three.

Both the KF and IMM-CT trackers were applied to the Es estimates, with results in Fig. 12. A localization error of below 5 m is achieved initially, and it seems that the tracking algorithms smooth out the small sample set, but offer no drastic improvement over the raw measurements.

C. Test Case 3

(Mobile test, December 2010)

For the moving test in the pool, a simple straight-line maneuver was carried out. All of the previous conditions apply from the stationary pool test, including the use of only three nodes for localizing purposes. There was a significant upgrade in the hardware and software used for the second test, which resulted in a large reduction in the overall error.

VI. Conclusion

In this paper, we presented an underwater localization solution based on one-way message broadcasting from multiple surface nodes. In addition to simulation results, we provided preliminary testing results in a swimming pool and in a local lake. Future work would involve large-scale field tests, and also accommodate mobile underwater nodes in addition to stationary nodes.

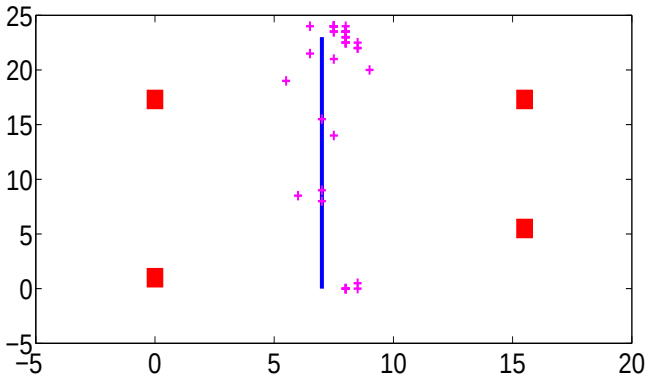

Fig. 13. Localization error in the swimming pool.

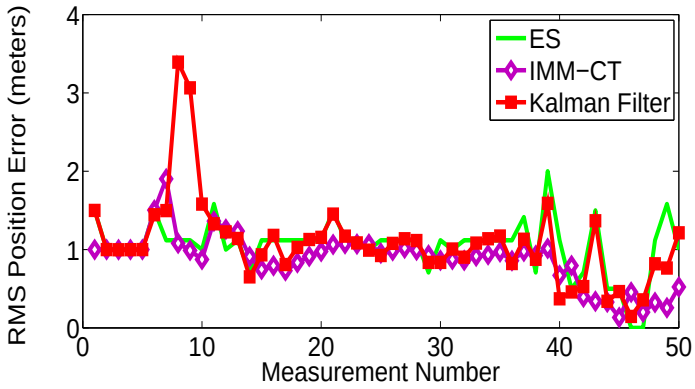

Fig. 14. Localization error in the swimming pool.

REFERENCES

[1] R. Stuart, “Acoustic Digital Spread Spectrum: An Enabling Technology,” *Sea Technology*, vol. 46, no. 10, Oct. 2005.

[2] C. Bechaz and H. Thomas, “GIB system: The underwater GPS solution,” in *Proceedings of ECUA*, May 2001.

[3] A. Caiti, A. Garulli, F. Livide, and D. Prattichizzo, “Localization of autonomous underwater vehicles by floating acoustic buoys: a set-membership approach,” *IEEE Transactions on Oceanic Engineering*, vol. 30, no. 1, pp. 140–152, Jan. 2005.

[4] H. Yan, S. Zhou, Z. Shi, J.-H. Cui, L. Wan, J. Huang, and H. Zhou, “DSP implementation of SISO and MIMO OFDM acoustic modems,” in *Proc. of MTS/IEEE OCEANS Conference*, Sydney, Australia, May 2010.

[5] S. Mason, C. R. Berger, S. Zhou, and P. Willett, “Detection, synchronization, and Doppler scale estimation with multicarrier waveforms in underwater acoustic communication,” *IEEE Journal on Selected Areas in Communications*, vol. 26, no. 9, pp. 1638–1649, Dec. 2008.

[6] D. A. Abraham and P. K. Willett, “Active Sonar detection in shallow water using the Page Test,” IEEE J. Ocean. Eng., vol. 27, no. 1, pp. 35–46, Jan. 2002.

[7] G. Mellen II, M. Pachter, and J. Raquet, ”Closed-form solution for determining emitter location using time difference of arrival measurements,” *IEEE Trans. Aerosp. Electron. Syst*, vol. 39, no. 3, pp. 10561058, 2003.

[8] B. Ferreira, A. Matos, and N. Cruz, “Estimation Approach for AUV Navigation Using a Single Acoustic Beacon,” *Sea Technology*, vol 51, no. 12, pp 54-58, Dec 2010.

[9] H. Wang, T. Kirubarajan, and Y. Bar-Shalom, “Precision Large Scale Air Traffic Surveillance Using IMM Estimator with Assignment,” *IEEE Trans. Aerospace and Electronic Systems*, pp 255-266, Jan. 1999.

[10] Y. Bar-Shalom, X. Rong Li, and T. Kirubarajan, *Estimation with Applications to Tracking and Navigation*, New York: John Wiley & Sons, Inc, 2001.